Capturing distinct KCNQ2 channel resting states by metal ion bridges in the voltage-sensor domain

Orit Gourgy-Hacohen,[1]* Polina Kornilov,[1]* Ilya Pittel,[2] Asher Peretz,[1] Bernard Attali,[1] and Yoav Paas[2]

[1]Department of Physiology and Pharmacology, Tel Aviv University, Tel Aviv 69978, Israel
[2]The Mina and Everard Goodman Faculty of Life Sciences, Institute of Nanotechnology and Advanced Materials, Bar-Ilan University, Ramat Gan 52900, Israel

Although crystal structures of various voltage-gated K^+ (Kv) and Na^+ channels have provided substantial information on the activated conformation of the voltage-sensing domain (VSD), the topology of the VSD in its resting conformation remains highly debated. Numerous studies have investigated the VSD resting state in the Kv *Shaker* channel; however, few studies have explored this issue in other Kv channels. Here, we investigated the VSD resting state of KCNQ2, a K^+ channel subunit belonging to the KCNQ (Kv7) subfamily of Kv channels. KCNQ2 can coassemble with the KCNQ3 subunit to mediate the I_M current that regulates neuronal excitability. In humans, mutations in KCNQ2 are associated with benign neonatal forms of epilepsy or with severe epileptic encephalopathy. We introduced cysteine mutations into the S4 transmembrane segment of the KCNQ2 VSD and determined that external application of Cd^{2+} profoundly reduced the current amplitude of S4 cysteine mutants S195C, R198C, and R201C. Based on reactivity with the externally accessible endogenous cysteine C106 in S1, we infer that each of the above S4 cysteine mutants forms Cd^{2+} bridges to stabilize a channel closed state. Disulfide bonds and metal bridges constrain the S4 residues S195, R198, and R201 near C106 in S1 in the resting state, and experiments using concatenated tetrameric constructs indicate that this occurs within the same VSD. KCNQ2 structural models suggest that three distinct resting channel states have been captured by the formation of different S4–S1 Cd^{2+} bridges. Collectively, this work reveals that residue C106 in S1 can be very close to several N-terminal S4 residues for stabilizing different KCNQ2 resting conformations.

INTRODUCTION

KCNQ channels (Kv7) comprise a subfamily of voltage-gated K^+ (Kv) channels that play important functions in different tissues including various epithelia, smooth muscle, brain, and heart (Maljevic et al., 2008; Peroz et al., 2008). In the brain, the KCNQ2 subunit coassembles with KCNQ3 to generate the I_M current, a slowly activating, noninactivating Kv current. The I_M current has profound effects on neuronal excitability, as its low threshold gating and slow activation act as a brake for repetitive firing (Delmas and Brown, 2005). In humans, mutations in KCNQ2 are associated with benign neonatal forms of epilepsy or with severe epileptic encephalopathy (Maljevic et al., 2008; Soldovieri et al., 2011; Weckhuysen et al., 2012). Like in all Kv channels, KCNQ2 α subunits possess two transmembrane modules: a pore-lining region and a voltage-sensing domain (VSD). VSDs are endowed with charged amino acids, also called gating charges. It is commonly recognized that four highly conserved arginine residues along S4 (R1, R2, R3, and R4) mainly contribute to the voltage-driven gating charge transfer during channel activation, which could be measured as gating currents (Armstrong and Bezanilla, 1974; Yellen, 1998; Swartz, 2004). The gating charges reside in aqueous crevices and translocate across a focused electric field, where hydrophobic residues form a plug that occludes the "gating pore" (Vargas et al., 2012). Along this narrow path, the positive charges in S4 are stabilized by electrostatic interactions with negative countercharges in segments S2 and S3, water dipoles in the crevices, and negatively charged phospholipids (Schmidt et al., 2006; Tao et al., 2010). Crystallographic studies of Kv1.2 channels and bacterial Na_vAb voltage-gated Na^+ channels have described the VSD architecture in its activated conformation (Jiang et al., 2003; Long et al., 2005, 2007; Payandeh et al., 2011). It is a module of four membrane-spanning segments (S1–S4), which moves at the protein–lipid interface (Long et al., 2007; Swartz, 2008). A portion of the S4 segment adopts a 3_{10}-helix conformation (Long et al., 2007; Payandeh et al., 2011). Although the activated

*O. Gourgy-Hacohen and P. Kornilov contributed equally to this paper. Correspondence to Yoav Paas: paasyo@mail.biu.ac.il; or Bernard Attali: battali@post.tau.ac.il

Abbreviations used in this paper: CHO, Chinese hamster ovary; Cu-Phen, copper phenanthroline; DTT, dithiothreitol; HEK, human embryonic kidney; Kv, voltage-gated K^+; VSD, voltage-sensing domain.

The Rockefeller University Press $30.00
J. Gen. Physiol. Vol. 144 No. 6 513–527
www.jgp.org/cgi/doi/10.1085/jgp.201411221

conformation of the VSD was elucidated from the crystal structures of different K^+ and Na^+ channels (Jiang et al., 2003; Long et al., 2005, 2007; Payandeh et al., 2011), its topology in the resting state has not yet been determined at atomic resolution and remains highly debated. Voltage-clamp fluorometry, cysteine cross-linking, and metal bridge experimental constraints were extensively used in the *Shaker* channel to predict the VSD resting-state conformation of Kv channels (Catterall, 2010; Vargas et al., 2012; see also, Campos et al., 2007; Pathak et al., 2007; Lin et al., 2010, 2011; Henrion et al., 2012). However, very few studies have addressed this issue in other Kv channels (Jensen et al., 2012; Xu et al., 2013). In this work, cysteine mutations S195C, R198C, and R201C were introduced into the S4 segment of the KCNQ2 channel. This approach was taken to potentially form metal bridges or covalent disulfide bonds with an endogenous cysteine in S1, upon external application of Cd^{2+} ions or copper phenanthroline (Cu-Phen), respectively. Electrophysiological experiments disclose the formation of three discrete S4–S1 Cd^{2+} bridges whose structural models infer the existence of three distinct KCNQ2 channel resting states.

MATERIALS AND METHODS

Constructs and mutagenesis

For expression in mammalian cells, KCNQ2 WT (provided by T. Jentsch, Leibniz-Institut für Molekulare Pharmakologie and Max-Delbrück-Centrum für Molekulare Medizin, Berlin, Germany) in pcDNA4/myc-His vector was used as a basic template. Site-directed mutagenesis was generated by PCR amplification using complementary mutagenic oligonucleotides (Hylabs) and Pfu polymerase (Promega). Mutant constructs were verified by DNA sequencing. For expression in *Xenopus laevis* oocytes, WT KCNQ2 was inserted into the PTLN vector, which was linearized by Mlu1. Capped complementary RNAs (cRNAs) were transcribed by SP6 RNA polymerases (Promega) and quantified by UV spectrophotometry (Nanodrop), and their integrity was verified on formaldehyde agarose gels. The WT KCNQ2 concatenated tetrameric construct was built into the pGEM vector using the same strategy described for KCNQ1 tetramers (Meisel et al., 2012), where subunits D1, D2, D3, and D4 were connected by flexible linkers of eight glycines, each harboring unique restriction sites BamHI, EcoRI, and EcoRV, respectively. The concatenated construct was confined by HindIII and XbaI restriction sites upstream and downstream, respectively. Using this cassette, each subunit could be removed and mutated separately by cut and paste with a pair of restriction enzymes. For example, the D1 subunit could be cut and pasted using HindIII and BamHI restriction enzymes. The concatenated KCNQ2 was then inserted into the pcDNA3 vector to allow expression in mammalian cells.

Cell cultures, transfection, and Western blotting

Chinese hamster ovary (CHO) cells were grown at 37°C in a humidified atmosphere with 5% CO_2. Cell cultures were maintained in Dulbecco's modified Eagle's medium supplemented with 2 mM glutamine, 10% fetal calf serum, and antibiotics. For electrophysiology, CHO cells were seeded on poly-D-lysine–coated glass coverslips and transfected using TransIT LT1 (Mirus) or jetPEI (Polyplus Transfection) with 0.5 µg pIRES-CD8 as a marker for transfection and with KCNQ2 WT or its mutants (0.5–1.5 µg). Transfected cells were visualized ∼40 h after transfection, using anti-CD8 antibody-coated beads. For Western blotting, human embryonic kidney (HEK) cells (HEK 293) were grown as CHO cells and transfected using the calcium phosphate method. Cells were washed in PBS and lysed with a buffer containing 50 mM Tris-HCl, pH 7.5, 150 mM NaCl, 0.1% Triton X-100, 1 mM EDTA, 1 mM PMSF, and a protease inhibitor cocktail (Sigma-Aldrich) for 1 h at 4°C under rotation. Cell lysates were cleared by centrifugation (10,000 *g* for 15 min at 4°C). Equal amounts of lysate proteins were resolved by 8% SDS-PAGE, and blots were reacted using rabbit anti-KCNQ2 antibodies (Alomone Labs).

Channel expression in *Xenopus* oocytes

Pieces of the ovary from female *Xenopus* frogs were surgically removed and digested with 1 mg/ml collagenase (type IA; Sigma-Aldrich) in Ca^{2+}-free ND96 for about 2 h to remove follicular cells. Stage V and VI oocytes were selected for cRNA injection and maintained at 18°C in ND96 (mM: 96 NaCl, 2 KCl, 1.8 mM $CaCl_2$, 1 $MgCl_2$, and 5 HEPES, titrated to pH 7.5 with NaOH), supplemented with 1 mM sodium pyruvate and 50 µg/ml gentamycin. Homomeric expression of WT and mutant KCNQ2 was performed by injecting 40 nl per oocyte (5 ng cRNA) using a Nanoject injector (Drummond).

Electrophysiology

Whole-cell patch-clamp recordings. Recordings were performed using the whole-cell configuration of the patch-clamp technique, as described previously (Peretz et al., 2010). Signals were amplified using a patch-clamp amplifier (Axopatch 200A; Molecular Devices), sampled at 2 kHz and filtered at 800 Hz via a four-pole Bessel low-pass filter. Data were acquired using pCLAMP 9 software in conjunction with a DigiData 1322A interface (Molecular Devices). The patch pipettes were pulled from borosilicate glass (Warner Instruments) with a resistance of 3–7 MΩ. The content of the intracellular pipette solution was (mM): 130 KCl, 5 MgATP, 5 EGTA, and 10 HEPES, adjusted with KOH to pH 7.4 (290 mOsm). The content of the external solution was (mM): 140 NaCl, 4 KCl, 1.8 $CaCl_2$, 1.2 $MgCl_2$, 11 glucose, and 5.5 HEPES, adjusted with NaOH to pH 7.4 (310 mOsm). All cells, unless otherwise specified, were incubated for half an hour in 100 µM dithiothreitol (DTT) before experiments. Series resistances (8–15 MΩ) were compensated (75–90%) and periodically monitored.

Two-electrode voltage-clamp in Xenopus oocytes. Whole-cell currents were recorded using the standard two-electrode voltage clamp. The recordings were performed 3–6 d after cRNA microinjection. Recording electrodes were filled with 3 M KCl and had a resistance of 0.5–1 MΩ. Currents were recorded at room temperature (20–22°C) in bath solutions, as described previously (Gibor et al., 2004). The bath solutions consisted of ND96 containing 0.1 mM $CaCl_2$ either alone or with 1 mM DTT or 100 µM Cu-Phen (at a 1:3 ratio). All cells were incubated for half an hour in 100 µM DTT before experiments. Control recordings were performed in the absence of DTT. Data were sampled at 1-kHz frequency and low-pass filtered at 0.2 kHz. The currents were recorded using an amplifier (GeneClamp 500; Molecular Devices). Data acquisition and analysis were performed using pCLAMP 8 software and a Pentium personal computer in conjunction with a Digidata 1200 interface (Molecular Devices).

Data analysis

Data analysis was performed using the Clampfit program (pCLAMP 9; Molecular Devices), Excel (Microsoft), and Prism 5.0 (GraphPad Software). Leak subtraction was performed offline, using the pCLAMP 9 software, assuming that the channels are closed at −90 mV.

Chord conductance (G) was calculated by using this equation:

$$G = I/(V - Vrev),$$

where I corresponds to the current amplitude measured at the respective voltage. Vrev is the calculated reversal potential (−92 mV). G was estimated at various test voltages V, and then normalized to a maximal conductance value, Gmax. Activation curves were fitted by the Boltzmann equation:

$$G/Gmax = 1/\{1 + \exp[(V_{50} - V)/s]\},$$

where V_{50} is the voltage at which the current is half-activated, and s is the slope factor.

All data are expressed as mean ± SEM. Statistically significant differences were assessed by two-tailed unpaired Student's *t* test, assuming equal variances for comparing values of WT KCNQ2 and KCNQ2 mutants. Results were considered significant for $P < 0.05$.

Structural modeling of the KCNQ2 channel closed states

We used comparative (homology) modeling techniques to produce 3-D model structures for the transmembrane segments and their flanking sequences of the human KCNQ2 K^+ channel (Swiss-Prot accession no. O43526). To this end, the sequence extending from A92 to H324 was submitted for searching a homologous template in the SWISS-MODEL repository, a database for theoretical protein models. The search for homologous sequences of known 3-D structures scored three known atomic resolution structures as potential templates, as follows. (1) The nuclear magnetic resonance structure of the KcsA K^+ channel (Protein Data Bank [PDB] accession no. 2K1E; chain B; Ma et al., 2008), which shares 37% sequence identity with residues 245–324 of KCNQ2. (2) The x-ray crystal structure of the Kv1.2 K^+ channel (PDB accession no. 2A79; chain B; Long et al., 2005), which shares 26% sequence identity with residues 166–324 of KCNQ2. (3) The x-ray crystal structure of the Kv1.2–Kv2.1 chimeric K^+ channel (PDB accession no. 2R9R; chain H; Long et al., 2007), which shares 22% sequence identity with residues 93–323 of KCNQ2. Among the three potential templates, the search scored 2r9rH with the lowest E-value (1.1E-44 compared with 4.5E-21 and 1.1E-36 for 2k1eB and 2a79B, respectively). Therefore, an initial model was built on the basis of the x-ray crystal structure of the Kv1.2–Kv2.1 chimeric K^+ channel, and was used as a starting point for building model structures for the resting states. 3-D alignment of the KCNQ2 homology model with the Kv1.2–Kv2.1 x-ray crystal structure showed root-mean-square deviation (RMSD) of 0.17 Å for 214 Cα atoms of the amino acids underlined in Fig. S5. The single-chain 3-D alignment was used to oligomerize four modeled chains around the axis of fourfold symmetry of Kv1.2–Kv2.1 to get a tetrameric open-state KCNQ homology model. We then rigidly pivoted the lower half of the S6 segments around their hinges at the level of P308 so as to eliminate lateral openings between adjacent S6 segments along the lower half of the open pore surface (at the level of A309 and G310) and to optimize the van der Waals interactions between adjacent S6 segments. Note that this rigid body movement caused ∼1.7-Å deviation at the level of the Gln323-Cα atom, with zero deviation at the level of the L307-Cα atom. We further optimized the model to eliminate steric clashes at the intersubunit interfaces by choosing nonclashing rotamers with COOT (Emsley et al., 2010) and performing energy minimization in vacuo to the entire tetrameric model structure using GROMOS96.

To derive the C3 (deep), C2 (intermediate), and C1 (superficial) closed (resting) states, three structural elements of chain A of the open-state model structure were modified. These are the VSD, the S4–S5 linker, and the S6 segment. In the VSD, a portion of the S4 segment was found to adopt a 3_{10}-helix conformation in the x-ray structures of the resting state of the MlotiK1 CNG channel, the active/relaxed state of the Kv1.2–Kv2.1 chimeric K^+ channel, and the preopen state of the NavAb Na^+ channel (Long et al., 2007; Clayton et al., 2008; Payandeh et al., 2011). Hence, similar to the approach taken by Henrion et al. (2012) for a *Shaker* channel, we introduced a nearly constant length of 3_{10}-helix conformation "sliding" along the S4 segment across all KCNQ2-state models, which allows for rotation of the S4 outer end only, without net free energy cost. In the resting C3, C2, C1, and open O states, the 3_{10} helix spans KCNQ2 residues 197–203, 201–207, 203–213, and 205–214, respectively (Fig. S5 B). For modeling the VSDs, S195, R198, or R210 were mutated in silico to a cysteine residue in C3, C2, or C1, respectively. To bring C195, C198, and C201 of each model sufficiently close to form a reversible Cd^{2+} bridge with C106 in S1 (center-to-center distance of 4.5–6.0 Å between the sulfur atoms), the S4 segment of chain A was translated downward (toward the intracellular side), similarly to what has been performed for the hypothetical closed-channel model of the Kv1.2–Kv2.1 chimeric K^+ channel (Long et al., 2007). Together with the downward translation, the S4 segment was rotated counterclockwise. In each model, this downward movement was further constrained by keeping the side chains of the residues carrying the gating charges in a distance that would allow the formation of salt bridges or hydrogen bonds with counterpart glutamate residues in S2. These pairs are: for C3, R198-E130 and R201-E140; for C2, R201-E130 and Q204-E140; for C1, Q204-E130 and R207-E140. This process resulted in the distances provided in Fig. 8 B and placed the C terminus of S4 in different topological levels: the lowest (deepest) position for C3, the highest (superficial) position for C1, and an intermediate position for C2. To connect the S4–S5 helical linker to S4 in the C3, C2, and C1 models, the linker was rigidly pivoted around the kink at its borderline with S5 (His228, Ser229), downward and toward the fourfold axis of symmetry. Concomitantly, the lower half of S6 was rigidly pivoted around P308 downward and toward the axis of fourfold symmetry, while maintaining the multiple van der Waals interactions of the S4–S5 helical linker with residues in the lower half of the S6 segment. Note that the shape of S6 in the closed states (segment W288–E322) turned out to be very similar (although not identical) to that of KcsA (PDB accession no. 1BL8; Doyle et al., 1998).

Before the oligomerization process, the single-chain models were subjected to validation in the RCSB PDB Validation Server under "Option 1" to run geometric checks outside of the deposition pipeline and to find violations in terms of close contacts, bond deviations, and covalent bond distances and angles. Subsequently, clashes have been eliminated by choosing low energy side-chain conformations using COOT, whereas other violations have been minimized by using COOT in combination with segmental in vacuo energy minimization with GROMOS96. Note that this process was also performed for chain A of the open-state model. To create tetrameric model structures for the closed states, chain A of each model was oligomerized around the axis of fourfold symmetry. To this end, the fold of the T234-F304 sequence of four A chains was superimposed, one at the time, on the same fold of the four chains of the open-state model structure (RMSD for the 284 backbone atoms is 0). A few clashes at the intersubunit interfaces were relieved by choosing low energy side-chain conformations.

All four final tetrameric models were subjected to geometry validation by SFCHECK at the RCSB PDB Validation Server under "Option 2." No issues have been found in terms of atomic clashes, peptide linkage, covalent geometry, chirality errors, and Phi/Psi torsion angles.

Notably, the Voronoi diagrams generated for the pore molecular surface of the three closed-state model structures (Fig. 7, A–C) indicate that the models' water-filled cavities share similar shape and dimensions, with a maximum diameter of ∼10 Å (Petřek et al.,

2007; Berka et al., 2012). This is also the diameter of the water-filled cavity in the open-channel model, but in this case, the water-filled cavity extends toward the intracellular side because of the concerted swinging of the lower half of the S6 segments away from the axis of fourfold symmetry. It should be noted that, below the water-filled cavity, the pore's molecular surface of the closed states greatly differs from that of the KcsA K^+ channel because of sequence dissimilarities and slightly different angle relatively to the axis of fourfold symmetry. In the KCNQ2 closed-state models, A309, G310, G313, and S314 line the pore between the water-filled cavity and the activation gate (A317). The homologous positions in KcsA are equipped with bulkier side chains (see Fig. S5 C). Hence, at these positions in KcsA (particularly T107 and A111), the pore looks much narrower than in the closed-state models whose pore lining at that region adopts an inverted cone shape.

Online supplemental material

The online supplemental material contains five figures. Fig. S1 shows the effects of Cd^{2+} ions and DTT on WT KCNQ2 expressed in CHO cells. Fig. S2 shows the effects of Cd^{2+} ions on endogenous KCNQ2 cysteine mutants C106A and C242A expressed in CHO cells. Fig. S3 shows the closed-state dependence of Cd^{2+} inhibition of S195C and R198C mutants expressed in CHO cells. Fig. S4 shows the effects of Cu-Phen on KCNQ2 S4 mutants S195C, R198C, and R201C expressed in *Xenopus* oocytes. Fig. S5 shows the sequence alignments of KCNQ2 and Kv1.2–Kv2.1 channels. The atomic coordinates of the KCNQ2 model structures are also provided in the online supplemental material, with the file names "KCNQ2_C3_mdl," "KCNQ2_C2_mdl," "KCNQ2_C1_mdl," and "KCNQ2_Open_mdl." Online supplemental material is available at http://www.jgp.org/cgi/content/full/jgp.201411221/DC1.

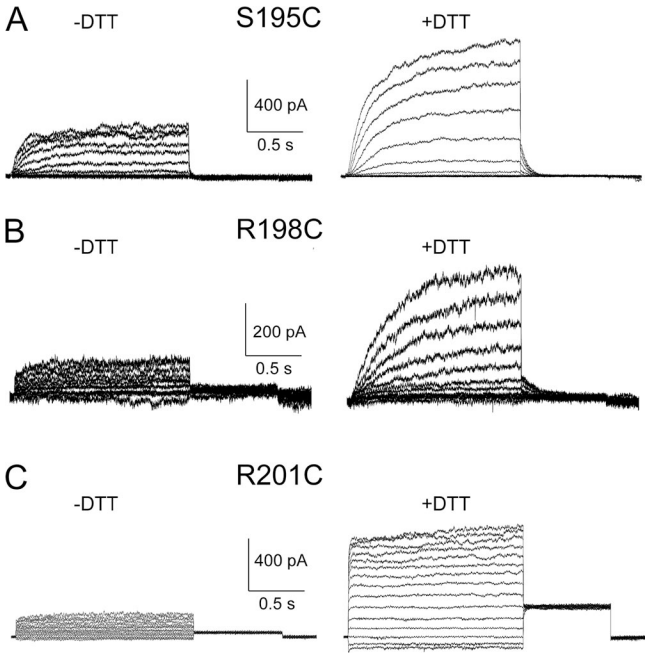

Figure 1. Effects of DTT on the KCNQ2 S4 mutants S195C, R198C, and R201C expressed in CHO cells. (A) Representative current traces (out of seven) of mutant S195C in the absence or presence of 100 µM DTT. Currents were evoked from a holding potential of −90 mV by depolarizing steps from −110 to 30 mV in 10-mV increments and repolarized to −60 mV. (B) Representative current traces (out of eight) of mutant R198C in the absence or presence of 100 µM DTT. Currents were evoked as in A. (C) Representative current traces (out of seven) of mutant R201C in the absence or presence of 100 µM DTT. Currents were evoked as in A.

RESULTS

Mutants S195C, R198C, and R201C in S4 are stabilized in the closed state after external Cd^{2+} application

In principle, if two externally accessible cysteines are close enough to each other, they should be able to form metal bridges or covalent disulfide bonds after external application of Cd^{2+} ions or Cu-Phen, respectively, and thereby modify ion channel activity. The WT KCNQ2 subunit has 16 endogenous cysteines, but only two are accessible from the external milieu and can potentially engage into metal bridge formation. These are C106 in S1, which is conserved in all KCNQ channel subtypes, and C242 in S5, which is exclusively present in KCNQ2. We initially introduced single cysteine mutations into segment S4 of the KCNQ2 subunit and compared the propensity of WT and mutant KCNQ2 channels to form metal bridges after the external application of 100 µM Cd^{2+}. To this end, channels were expressed in CHO cells, and currents were recorded using the whole-cell configuration of the patch-clamp technique.

WT KCNQ2 displayed no significant differences in V_{50} or current amplitude after the external application of 100 µM Cd^{2+} ($CdCl_2$) (Fig. S1, A–C, and Table 1) or 100 µM DTT (Fig. S1, D–F). A slight decrease in current amplitude was observed even after washout, which probably reflects minor current rundown caused by a decrease in membranous PIP_2 (Li et al., 2005). This suggests that none of the endogenous cysteine in WT KCNQ2 is able to form a metal bridge under these experimental conditions, or alternatively, if any bridge is formed, it does not affect channel function.

Recording of the S4 mutants S195C, R198C, and R201C without DTT resulted in very small currents (Fig. 1, A–C, left, -DTT). In contrast, a large increase in current amplitudes (two- to fivefold) was observed after external exposure of cells to 100 µM DTT for ∼15 min (Fig. 1, A–C, right, +DTT). This implies that in mutants S195C, R198C, and R201C, disulfide bonds probably form spontaneously and stabilize the channels in their closed state. Thus, to prevent spontaneous disulfide bond formation and to study the effects of Cd^{2+} on S4 mutants, CHO cells were routinely preincubated for 30 min with 100 µM DTT before recording experiments. Under these conditions, mutant R201C formed a constitutively open channel (Fig. 1 C). Mutants S195C and R198C exhibited a significant right-shift in their voltage dependence of activation when compared with WT (Table 1; compare Fig. 1, A and B, and Fig. 2, A–D, with Fig. S1, A–C). In addition, mutant R198C showed significantly slower activation kinetics when compared with WT (at 0 mV, for WT and R198C, respectively, half-time to peak $t_{1/2} = 0.15 \pm 0.02$ s, $n = 23$, and $t_{1/2} = 0.54 \pm 0.04$ s, $n = 7$, $P < 0.005$; Fig. 2 C).

In contrast to WT KCNQ2, mutants S195C, R198C, and R201C were highly responsive to externally added 100 µM Cd^{2+} (Fig. 2, A–F, and Table 1). They showed a dramatic reduction in current amplitudes, which was reversible upon extensive washout. The decrease in current amplitude was calculated as the ratio of normalized current after and before Cd^{2+} application at 30 mV and was expressed as I_{Cd}. All three cysteine mutants, S195C, R198C, and R201C, exhibited a significant, very low I_{Cd} ratio (Table 1). The IC_{50} for Cd^{2+} inhibition of mutant R198C was 10.9 ± 1.1 µM (Hill slope = 3.1; $n = 6$), suggesting a strong Cd^{2+} coordination. These results indicate that upon Cd^{2+} treatment, metal bridges were formed, thereby stabilizing the mutant channels in the closed-state conformation.

The endogenous cysteine 106 in S1 forms Cd^{2+} bridges with cysteines substituted in S4

Cd^{2+} bridges were shown previously to capture ion channels in physiologically relevant conformations, constraining distances of interacting cysteine C_β atoms to <6.5 Å and allowing for metal–sulfur interactions (Lainé et al., 2003; Webster et al., 2004; Campos et al., 2007; Henrion et al., 2012). At least two Lewis base ligands are required for proper coordination of Cd^{2+} ions, which can include cysteine, histidine as well as glutamate, and aspartate (Rulíšek and Vondrásek, 1998). To find the residue that is sufficiently close to coordinate Cd^{2+} with the S4 cysteine mutants S195C, R198C, and R201C, we mutated each of the two externally accessible endogenous cysteines into alanine, i.e., C106A in S1 and C242A in S5. When expressed alone, the two single mutants displayed a significant left-shift of their activation curve when compared with WT KCNQ2 (see Table 1). However, they showed no significant changes in their current amplitudes, gating parameters, and kinetics after Cd^{2+} exposure (Table 1 and Fig. S2).

Double mutations of C106A or C242A with the S4 mutants S195C, R198C, or R201C were examined. Our results indicate that a marked current inhibition was still observed after exposure to 100 µM Cd^{2+} in each of the three S4 double mutant channels, C242A-S195C, C242A-R198C, and C242A-R201C (Fig. 3, A and B, and Table 1). In contrast, a significant attenuation in the Cd^{2+} inhibitory effect was found in three double mutants, C106A-S195C, C106A-R198C, and C106A-R201C, when

TABLE 1

Effects of Cd^{2+} on the amplitude and voltage dependence of the various homomeric and heteromeric channels

Channel	V_{50}	V_{50Cd}	I_{Cd}[a]
	mV	*mV*	
WT Q2	−20.0 ± 2.3 (23)	−22.7 ± 2.4 (23)	0.80 ± 0.04 (23)
S195C Q2	1.4 ± 1.6[b] (7)	—	0.09 ± 0.02[b] (7)
R198C Q2	−0.8 ± 2.6[b] (7)	—	0.09 ± 0.02[b] (7)
R201C Q2	—	—	0.12 ± 0.02[b] (6)
C106A Q2	−35.2 ± 1.4[b] (5)	−35.9 ± 4.0[b] (5)	0.92 ± 0.10 (5)
C242A Q2	−31.1 ± 1.5[b] (6)	−29.8 ± 1.5[b] (6)	0.92 ± 0.04 (6)
C242A-S195C Q2	−6.8 ± 0.7 (7)	—	0.10 ± 0.03[b] (7)
C242A-R198C Q2	5.2 ± 0.3 (6)	—	0.07 ± 0.01[b] (6)
C242A-R201C Q2	—	—	0.12 ± 0.02[b] (5)
C106A-S195C Q2	−15.2 ± 0.5 (5)	−28.9 ± 1.1 (5)	0.64 ± 0.05[c] (5)
C106A-R198C Q2	−9.4 ± 0.3[b] (5)	−22.3 ± 0.3 (5)	0.71 ± 0.08[c] (5)
C106A-R201C Q2	—	—	0.72 ± 0.07[c] (5)
WT Q2/WT Q3	−34.3 ± 4.3 (7)	−32.4 ± 4.2 (7)	0.98 ± 0.21 (7)
R198C Q2/WT Q3	−18.8 ± 1.5[b] (7)	—	0.16 ± 0.05[b] (7)
C106A-R198C Q2/WT Q3	−23.8 ± 3.8[b] (6)	−25.3 ± 3.5[b] (6)	0.97 ± 0.03 (6)
R198C Q2/C136A Q3	−12.2 ± 0.3[b] (7)	—	0.28 ± 0.07[b] (7)
WT Q2/C136A Q3	−38.8 ± 3.0 (6)	−40.1 ± 3.2 (6)	0.96 ± 0.14 (6)
Con WT Q2	−26.3 ± 1.3 (7)	−24.6 ± 1.7 (7)	0.99 ± 0.05 (7)
Con Q2 D1 R198C	−19.4 ± 0.7[b] (7)	−25.7 ± 0.4 (7)	0.40 ± 0.06[b] (7)
Con Q2 D1 R198C, D2C106A	−21.1 ± 0.8 (7)	−30.6 ± 0.6 (7)	0.32 ± 0.05[b] (7)
Con Q2 D1 C106A, R198C	−23.8 ± 0.6 (7)	−25.5 ± 0.4 (7)	0.75 ± 0.16 (7)

In transfected CHO cells perfused without or with 100 µM Cd^{2+}, currents were evoked from a holding potential of −90 mV by depolarizing steps from −110 to 30 mV in 10-mV increments and repolarized to −60 mV. Conductance–voltage relations were constructed and data were fitted to a single Boltzmann function to yield the V_{50} values. The values in parentheses correspond to the number of cells examined. Data are expressed as mean ± SEM.
[a]The change in current amplitude was expressed as a ratio I_{Cd} of the current measured in the same cell at 30 mV after and before Cd^{2+} application.
[b]Statistically different from the WT KCNQ2 value, calculated by two-tailed unpaired Student's *t* test, assuming equal variances; $P < 0.01$.
[c]Statistically different from the single KCNQ2 mutant S195C, R198C, and R201C values; $P < 0.01$.

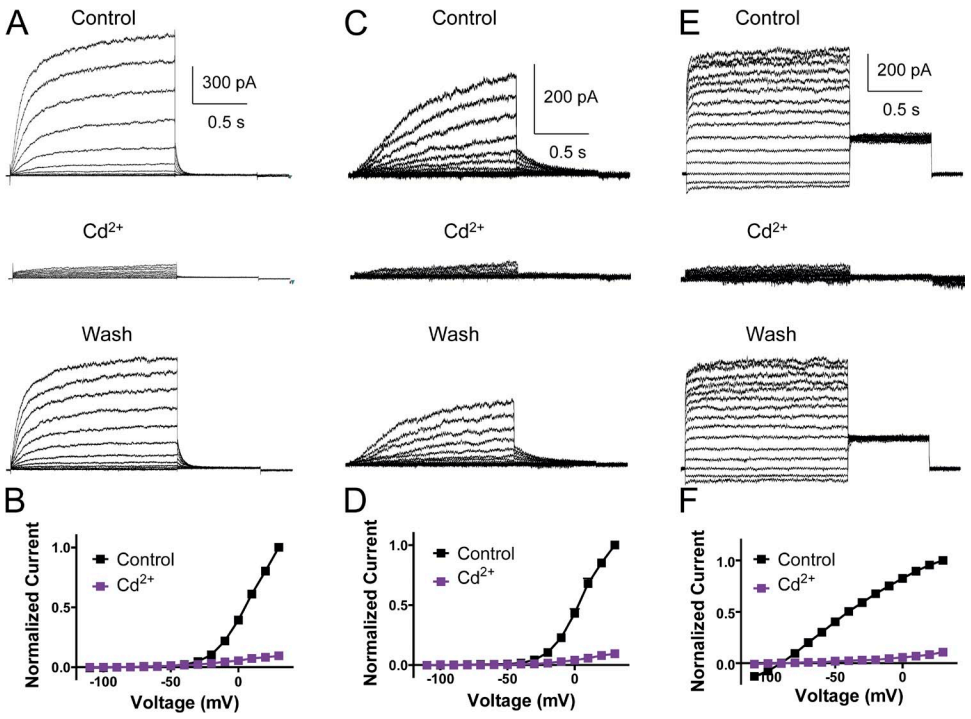

Figure 2. Effects of Cd^{2+} ions on the KCNQ2 S4 mutants S195C, R198C, and R201C expressed in CHO cells. (A) Representative current traces of mutant S195C in the absence (top) and presence of 100 µM Cd^{2+} (middle), and after washout (bottom). Currents were evoked as in Fig. 1 A. (B) Normalized current–voltage relations of mutant S195C in the absence and presence of 100 µM Cd^{2+} ($n = 7$). (C) Representative current traces of mutant R198C in the absence (top) and presence of 100 µM Cd^{2+} (middle), and after washout (bottom). (D) Normalized current–voltage relations of mutant R198C in the absence and presence of 100 µM Cd^{2+} ($n = 7$). (E) Representative current traces of mutant R201C in the absence (top) and presence of 100 µM Cd^{2+} (middle), and after washout (bottom). (F) Normalized current–voltage relations of mutant R201C in the absence and presence of 100 µM Cd^{2+} ($n = 6$).

compared with the single S4 mutants (Fig. 3, A and B, and Table 1). These results indicate that the substituting residues in mutants S195C, R198C, or R201C in S4 are constrained near C106 in S1.

The state dependence of metal bridges and disulfide bond formation

Coordination of Cd^{2+} by cysteines substituted in S4 and the native C106 in S1 may occur in the resting-state

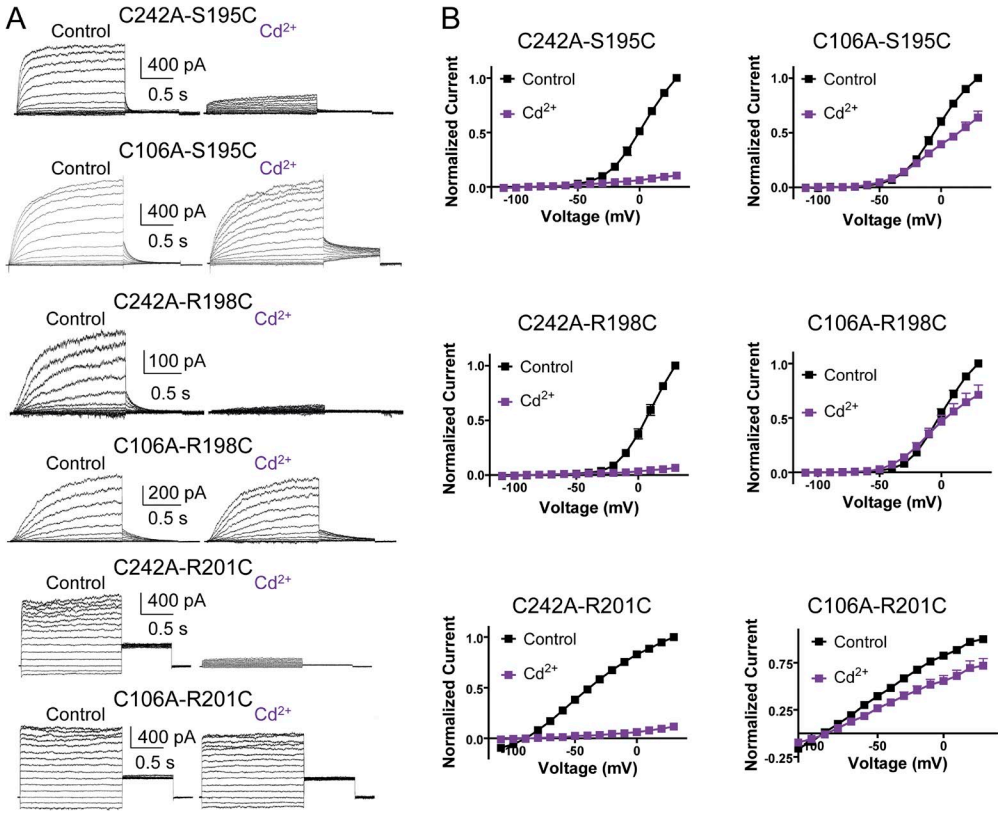

Figure 3. Effects of Cd^{2+} ions on the KCNQ2 S4–S5 and S4–S1 double mutants expressed in CHO cells. (A) From top to bottom rows, representative current traces of the indicated KCNQ2 S4–S5 and S4–S1 double mutants in the absence (left) or presence of 100 µM Cd^{2+} (right), and (B) their corresponding normalized current–voltage relations; $n = 5$–7. Currents were evoked as in Fig. 1 A. Error bars show mean ± SEM.

TABLE 2

Effects of Cu-Phen on the amplitude and voltage dependence of WT KCNQ2 and S4 cysteine mutants

Channel	V_{50}	V_{50}-Cu-Phen	$I_{Cu\text{-}Phen}$[a]
	mV	*mV*	
WT Q2	−32.2 ± 1.4 (10)	−29.5 ± 1.1 (10)	1.07 ± 0.11 (10)
S195C Q2	5.2 ± 4.0[b] (8)	0.8 ± 6.0[b] (8)	0.26 ± 0.06[b] (8)
R198C Q2	−31.0 ± 4.4 (7)	−5.3 ± 4.8 (7)	0.27 ± 0.06[b] (7)
R201C Q2	—	—	0.33 ± 0.07[b] (7)

Xenopus oocytes were incubated for 2 min at −80 mV in ND96 solution in the absence or presence of 100 µM Cu-Phen, washed with ND96 for another 5 min at −80 mV, and then depolarized from −90 to 45 mV in 15-mV increments and repolarized at −60 mV. Conductance–voltage relations were constructed and data were fitted to a single Boltzmann function to yield the V_{50} values. The values in parentheses correspond to the number of cells examined. Data are expressed as mean ± SEM.

[a]The change in current amplitude was expressed as a ratio $I_{Cu\text{-}Phen}$ of the current measured in the same cell at 45 mV after and before Cu-Phen application at −80 mV.

[b]Statistically different from the WT KCNQ2 value, calculated by two-tailed unpaired Student's *t* test, assuming equal variances; $P < 0.01$.

conformation, thereby preventing effective opening of the channel. Alternatively, Cd^{2+} ions may be coordinated in the open-state conformation and subsequently cause the channel to close. To determine the state dependence of metal bridge formation, we incubated the cells for 5 min with Cd^{2+} at −90 mV, a voltage at which the channel is closed, and then we checked the current amplitude at the first depolarizing pulse to 30 mV. If Cd^{2+} coordination occurs while the channel is in its closed-state conformation, we expect to see a strong reduction in current amplitude at the first depolarizing pulse as compared with the control current recorded in the same cell without Cd^{2+} pretreatment. Alternatively, if Cd^{2+} coordination occurs in the open-state conformation, we expect to see no change in current amplitude at the first depolarizing pulse compared with the control current, and eventually a strong decrease of the current amplitude after subsequent depolarization. After pretreatment with Cd^{2+} at −90 mV, both mutants S195C and R198C exhibited a dramatic and reversible reduction in current amplitude at the first depolarizing pulse to 30 mV compared with the control current recorded in the same cell without Cd^{2+} pretreatment (inhibition of 91 ± 3% and 90 ± 4% for S195C and R198C, respectively [$n = 6$], with $P < 0.01$ when comparing to without Cd^{2+} pretreatment; Fig. S3, A and B). This indicates that the Cd^{2+} bridges are likely to be formed in the channel closed state.

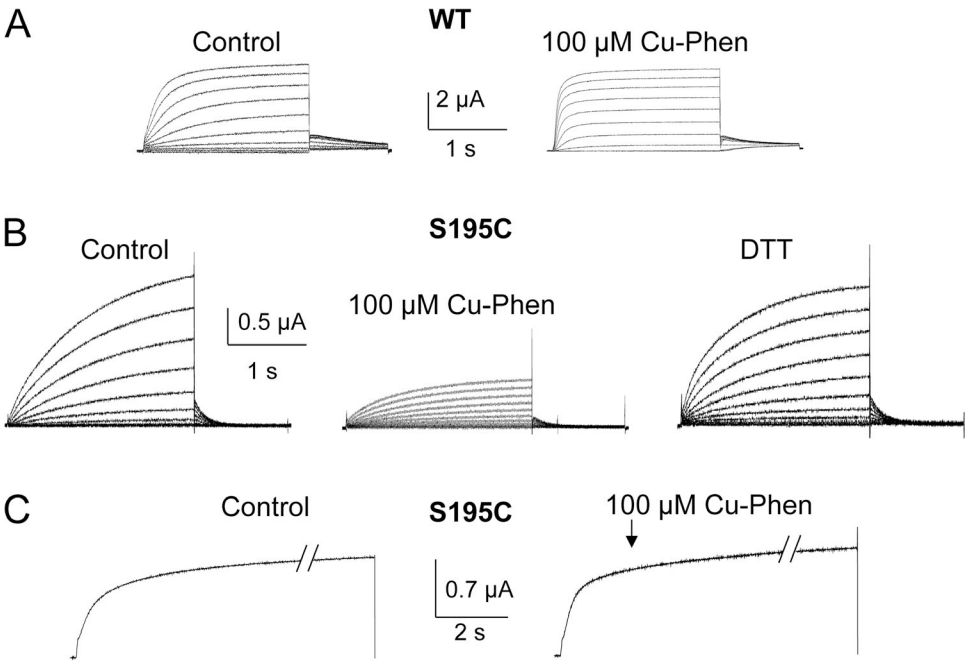

Figure 4. State dependence of disulfide bond formation in mutant S195C expressed in *Xenopus* oocytes. (A) Representative current traces of WT KCNQ2 in the absence or presence of 100 µM Cu-Phen; $n = 10$. At a holding potential of −80 mV, *Xenopus* oocytes were depolarized from −90 to 45 mV in 15-mV increments and repolarized at −60 mV. (B) Representative current traces of mutant S195C before or after Cu-Phen application in the channel closed state and after washout with 1 mM DTT. Oocytes were incubated for 2 min at −80 mV in ND96 solution containing 100 µM Cu-Phen, washed with ND96 for another 5 min at −80 mV, and then depolarized as in A; subsequently, the oocytes were washed out in the presence of 1 mM DTT and subjected to the same depolarizing protocol as in A; $n = 8$. (C) Representative current traces of mutant S195C before or after Cu-Phen application in the channel open state. From a holding potential of −80 mV, oocytes were subjected to a depolarizing step to 30 mV. 2 s after the beginning of the test pulse, fast application of 100 µM Cu-Phen was applied for up to 2 min; $n = 8$.

To support this notion, we explored the state dependence of disulfide bond formation using Cu-Phen, which catalyzes the covalent disulfide cross-link of closely located cysteines. We found that Cu-Phen is highly toxic for CHO cells; therefore, we conducted the experiments in *Xenopus* oocytes, which were incubated for 30 min in 100 µM DTT before experiments. External application of 100 µM Cu-Phen (at a 1:3 ratio) either at −80 mV or after repeated depolarization at 30 mV did not alter the current amplitude and the gating parameters of the WT KCNQ2 (Table 2 and Fig. 4 A).

To check the formation and the state dependence of disulfide bonds in the S4 cysteine mutants, we initially examined the propensity of each mutant, S195C, R198C, and R201C, to form covalent bonds after Cu-Phen application at a depolarizing membrane voltage, which reflects a channel open state. 2 s after the beginning of a test pulse to 0 mV (or 30 mV for the right-shifted mutant S195C), fast application of 100 µM Cu-Phen was applied for up to 2 min. If Cu-Phen catalyzes mutant channel disulfide covalent bond formation in the open state, one should expect a reduction in current amplitude during prolonged depolarization. We found that Cu-Phen had virtually no effect on S195C, R198C, and R201C mutant channels in their open-state conformation (Figs. 4 C and 5, B and D). The decrease in current amplitude, expressed as ratios $I_{Cu\text{-}Phen}$ of normalized current after and before Cu-Phen application at 0 mV, was as follows. For S195C, $I_{Cu\text{-}Phen}$ = 0.99 ± 0.03 (n = 8, P > 0.05); for R198C, $I_{Cu\text{-}Phen}$ = 0.94 ± 0.09 (n = 7, P > 0.05); and for R201C, $I_{Cu\text{-}Phen}$ = 0.95 ± 0.10 (n = 10, P > 0.05) (Figs. 4 C and 5, B and D).

To investigate the propensity of mutants S195C, R198C, and R201C to form covalent disulfide bonds at a hyperpolarizing membrane voltage, which reflects a channel closed state, we incubated the oocytes for 2 min at −80 mV in ND96 solution containing 100 µM Cu-Phen in the absence of DTT. Then, we washed the Cu-Phen with the ND96 solution for another 5 min at −80 mV and depolarized the oocyte membrane from −90 to 45 mV in 15-mV increments. Our results indicated a dramatic reduction in the current amplitude of all three mutants, S195C, R198C, and R201C, which could be reversed by external perfusion with 1 mM DTT (Figs. 4 B, 5, A and C, and S4). The significant decrease in current amplitudes was reflected by the very low $I_{Cu\text{-}Phen}$ ratios (see Table 2). Cu-Phen also produced a right-shift in the voltage dependence of R198C mutant channel activation (Table 2

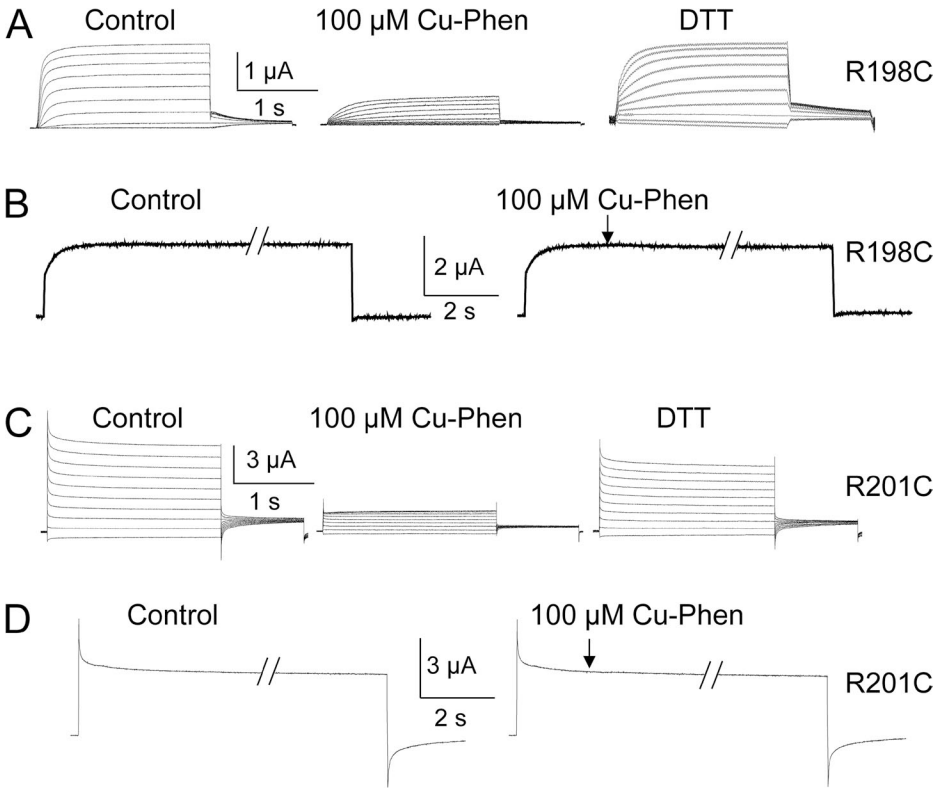

Figure 5. State dependence of disulfide bond formation in mutants R198C and R201C expressed in *Xenopus* oocytes. (A) Representative current traces of mutant R198C before or after Cu-Phen application in the channel closed state and after washout with 1 mM DTT. Oocytes were incubated for 2 min at −80 mV in ND96 solution containing 100 µM Cu-Phen, washed with ND96 for another 5 min at −80 mV, and then depolarized as in Fig. 4 A; subsequently, the oocytes were washed out in the presence of 1 mM DTT and subjected to the same depolarizing protocol; n = 7. (B) Representative current traces of mutant R198C before or after Cu-Phen application in the channel open state. From a holding potential of −80 mV, oocytes were subjected to a depolarizing step to 0 mV. 2 s after the beginning of the test pulse, fast application of 100 µM Cu-Phen was applied for up to 2 min; n = 7. (C) Representative current traces of mutant R201C before or after Cu-Phen application at −80 mV and after washout with 1 mM DTT. Oocytes were treated and currents were evoked as in Fig. 4 A; n = 7. (D) Representative current traces of mutant R201C before or after Cu-Phen application in the channel open state. Oocytes were treated and currents were evoked as in B; n = 10.

and Fig. S4). Collectively, the results suggest that covalent disulfide bonds are likely to form in the channel closed-state conformation between residues C195 in S4 and C106 in S1 for mutant S195C, and between residues C198 in S4 and C106 in S1 for mutant R198C. For the mutant R201C, although disulfide bonds probably form between residues C201 in S4 and C106 in S1 at hyperpolarized potentials, no state dependence could be deduced because this channel is constitutively open at all voltages.

Mutant R198C in S4 is constrained near C106 in S1 within the same VSD

To determine whether Cd^{2+} coordination between R198C in S4 and C106 in S1 occurs within the same monomer, or between two adjacent subunits, CHO cells were cotransfected with KCNQ2 (WT or mutant) and KCNQ3 (WT or mutant) subunits. These experiments could be performed because of the high sequence homology between KCNQ2 and KCNQ3 subunits, including the S1 and S4 segments. Notably, C106 in KCNQ2 S1 is highly conserved in the KCNQ family, corresponding to C136 in KCNQ3. Thus, WT KCNQ2/WT KCNQ3, R198C KCNQ2/WT KCNQ3, C106A-R198C KCNQ2/WT KCNQ3, R198C KCNQ2/C136A KCNQ3, and WT KCNQ2/C136A KCNQ3 heteromers were expressed in CHO cells (Fig. 6). Comparing the gating parameters of WT KCNQ2 (homomers) and of R198C KCNQ2 (homomers) with those of WT KCNQ2/WT KCNQ3 (heteromers) and R198C KCNQ2/WT KCNQ3 (heteromers) suggests that heteromers are likely to assemble properly in CHO cells (see Table 1). Similar conclusions could be drawn when comparing the activation kinetics of homomers and heteromers (at 0 mV, half-time to peak was $t_{1/2}$ = 0.15 ± 0.02 s [n = 23] and $t_{1/2}$ = 0.54 ± 0.04 s [n = 7] for WT KCNQ2 and R198C KCNQ2 vs. $t_{1/2}$ = 0.08 ± 0.02 s [n = 7] and $t_{1/2}$ = 0.17 ± 0.01 s [n = 7] for WT KCNQ2/WT KCNQ3 and R198C KCNQ2/WT KCNQ3, respectively).

The gating and current amplitude of the WT KCNQ2/WT KCNQ3 heteromer were unaffected by external application of 100 µM Cd^{2+} (Table 1 and Fig. 6, A and B, first row). Notably, the exposure to Cd^{2+} profoundly depressed the current amplitudes of R198C KCNQ2/WT KCNQ3 and R198C KCNQ2/C136A KCNQ3 heteromers (Table 1 and Fig. 6, A and B, second and fourth rows). In contrast, mutating the endogenous cysteine C106A in KCNQ2 S1 produced a significant decline in Cd^{2+} inhibition of the C106A-R198C KCNQ2/WT KCNQ3 heteromer as compared with the Cd^{2+} inhibitory effect on R198C KCNQ2/WT KCNQ3 or on R198C KCNQ2/C136A KCNQ3 heteromers (Table 1 and Fig. 6, A and B, third row). As a control, the WT KCNQ2/C136A KCNQ3 heteromer was unaffected by external application of 100 µM Cd^{2+} (Table 1 and Fig. 6, A and B, fifth row). These

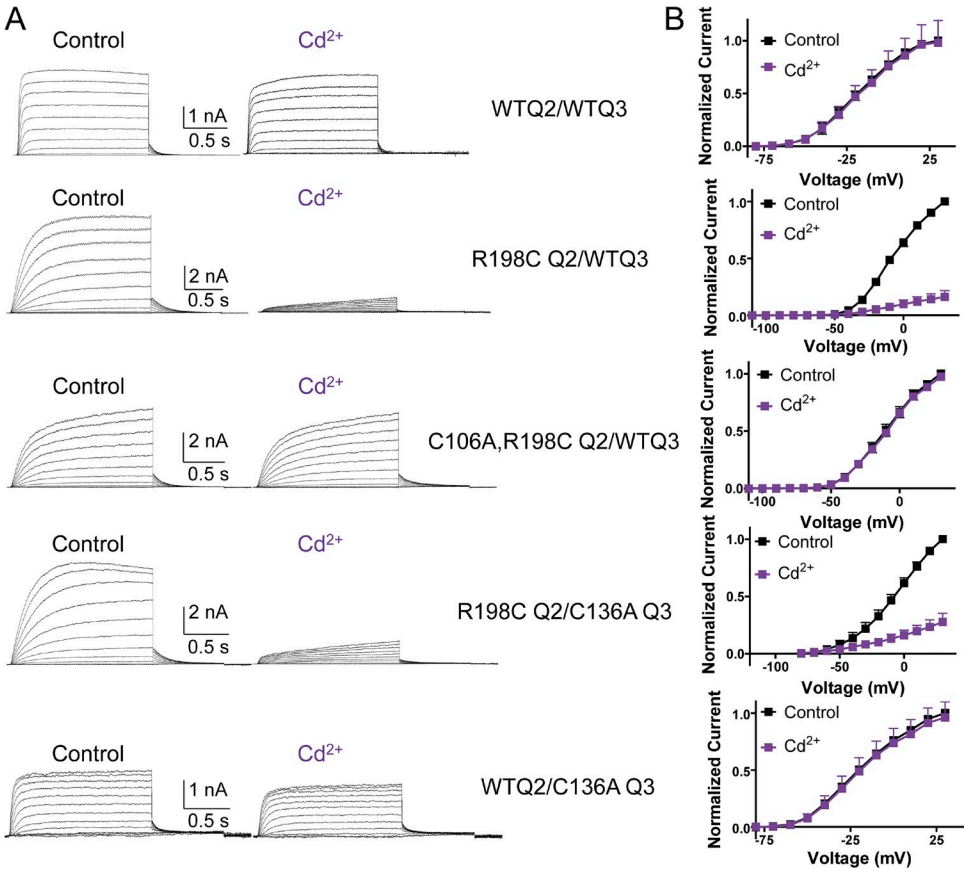

Figure 6. Sensitivity of S4 and S1 mutants to Cd^{2+} ions in KCNQ2/KCNQ3 heteromers expressed in CHO cells. (A) From top to bottom rows, representative current traces of the indicated KCNQ channel assemblies, in the absence (left) or presence of 100 µM Cd^{2+} (right) and (B) their corresponding normalized current–voltage relations; n = 6–23. Currents were evoked as in Fig. 1 A. Error bars show mean ± SEM.

data suggest that the substituting residue in S4 of mutant R198C is constrained near C106 of S1 within the same VSD.

To further substantiate this idea, we introduced the mutations R198C (in S4) and C106A (in S1) into the same or adjacent subunits of a concatenated tetrameric KCNQ2 channel. The WT and mutant KCNQ2 concatenated tetrameric constructs were built into a vector, where subunits D1, D2, D3, and D4 were connected by flexible linkers (eight glycines), each harboring unique restriction sites (Fig. 7 A), as described previously (Meisel et al., 2012). To ensure that our constructs were expressed as tetrameric channel proteins, we compared WT concatemer expression in HEK 293 cells with that of the monomeric KCNQ2 protein by examining its molecular weight in SDS-PAGE under reducing conditions followed by Western blotting. The monomeric KCNQ2 construct appeared as a main immunoreactive band of ∼90 kD accompanied by higher molecular weight bands, probably dimers and tetramers formed under denaturation conditions. In contrast, the concatemeric construct displayed a major high molecular weight immunoreactive band of >350 kD, which roughly corresponds to the tetrameric channel protein (Fig. 7 A). To validate the functional use of the concatemeric construct, the electrophysiological properties of the WT monomeric and WT concatemeric KCNQ2 constructs were compared in transfected CHO cells. The results indicate that the WT concatemeric KCNQ2 exhibits gating properties similar to those of the monomeric KCNQ2 construct (Table 1 and Fig. 7 B).

The WT concatemeric KCNQ2 was unaffected by external application of 100 µM Cd^{2+} (Table 1). However, when the S4 mutation R198C was created in subunit D1 alone (KCNQ2 concatemer D1 R198C), or in the presence of the S1 mutation C106A generated in the adjacent subunit D2 (KCNQ2 concatemer D1 R198C, D2 C106A), the application of 100 µM Cd^{2+} produced a large and significant inhibition of the current amplitude (Table 1 and Fig. 7, C–F). In contrast, when the S4 mutation R198C was created together with the S1 mutant C106A in the same D1 subunit (KCNQ2 concatemer D1 R198C, C106A), the application of 100 µM Cd^{2+} did not significantly affect the current amplitude (Table 1 and Fig. 7, G and H). Collectively, these data confirm our suggestion that in the channel closed state, R198 in S4 is close to C106 in S1 within the VSD of the same subunit.

DISCUSSION

Except for the most recently described resting-state structure of the voltage-gated proton channel mHv1 (Takeshita et al., 2014), all crystal structures of different

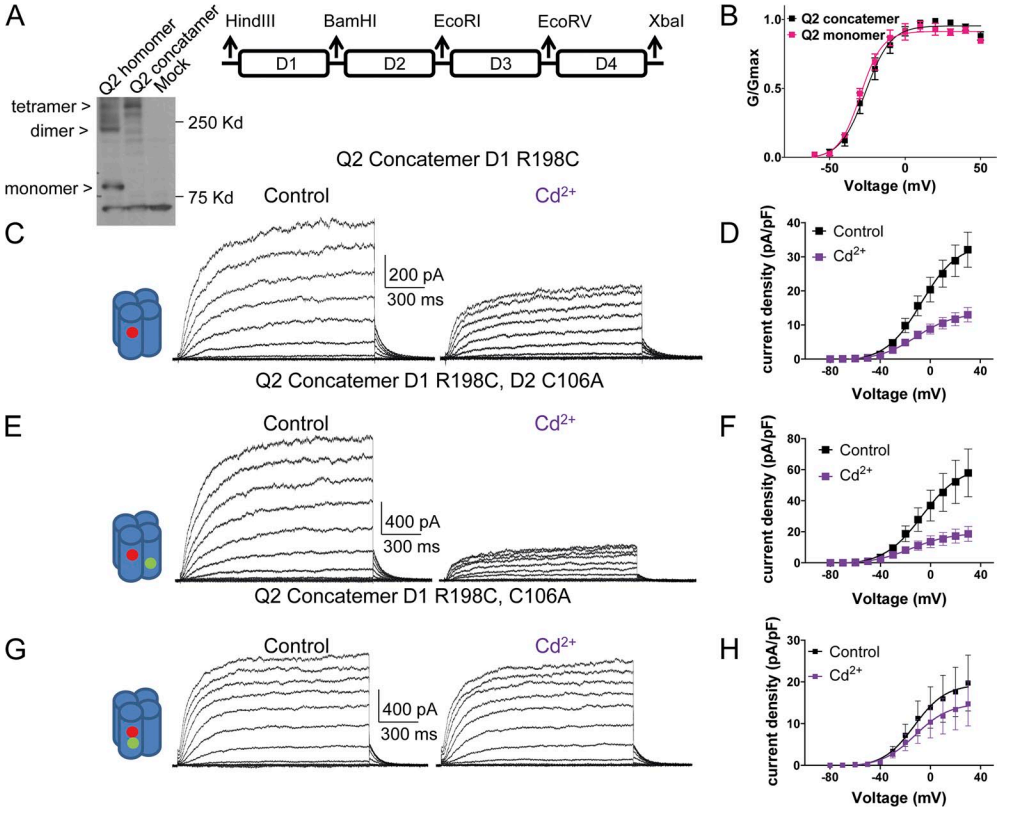

Figure 7. Effects of Cd^{2+} ions on concatenated tetrameric KCNQ2 mutants expressed in CHO cells. (A; right) Scheme of the KCNQ2 concatenated tetrameric channel construct, where subunits D1, D2, D3, and D4 are connected by flexible linkers. Each linker (eight glycines) harbors a unique restriction site. (Left) Western blot showing lysates of HEK 293 cells transfected with empty vector (Mock) and KCNQ2 monomeric and concatenated tetrameric constructs. (B) Conductance–voltage relations of WT monomeric and WT concatenated tetrameric KCNQ2 constructs. Data were fitted to a single Boltzmann function. (C and D) Representative current traces of KCNQ2 concatemer D1 R198C mutant in the absence or presence of 100 µM Cd^{2+} and corresponding current density–voltage relations; $n = 7$. (E and F) Representative current traces of KCNQ2 concatemer D1 R198C, D2 C106A in the absence or presence of 100 µM Cd^{2+} and corresponding current density–voltage relations; $n = 7$. (G and H) Representative current traces of KCNQ2 concatemer D1 R198C, C106A in the absence or presence of 100 µM Cd^{2+} and corresponding current density–voltage relations; $n = 7$. Error bars show mean ± SEM.

Kv and voltage-gated Na^+ channels have captured the VSD in its activated conformation (Jiang et al., 2003; Long et al., 2005, 2007; Payandeh et al., 2011). Thus, the VSD resting-state conformation has been the focus of intense experimental and modeling work. Most of the experimental and modeling studies were performed in *Shaker* channels and to a lesser extent in Kv1.2 (Jensen et al., 2012); however, attempts to predict the VSD resting state in other Kv channels are very limited (Haitin et al., 2008; Xu et al., 2008, 2013; Van Horn et al., 2011). Here, we aimed to address this issue in KCNQ2 channels. Structural homology models of KCNQ1 in the closed-state conformation were developed previously (Smith et al., 2007; Kang et al., 2008; Van Horn et al., 2011). However, initial attempts to derive a resting-state model of KCNQ2, based on the previously published model of KCNQ1, failed because it did not fit with all of our experimental constraints (Smith et al., 2007; Kang et al., 2008; Van Horn et al., 2011). This is probably because KCNQ channels display more than one closed state. To overcome this limitation, three distinct closed-state models of KCNQ2 were constructed by applying each of our Cd^{2+} bridge constraints (Figs. 8, A–F, and 9, A–C). These closed-state models were built by using the crystal structure of the open/relaxed state of the Kv1.2–Kv2.1 chimera (Long et al., 2007) as a starting point, and by making the following assumptions: (a) The topologies of S4 and S1 in the models are constrained by our experimental data, such that each closed state—C195, C198, or C201 in S4—is in atomic proximity to C106 in S1. (b) The S4–S5 linker was kept in contact with the C terminus of the S6 segment, such that the intracellular gate remained closed. (c) The S1 and S2 segments do not move during the closed to open transition. (d) The atomic distance between two sulfhydryls was constrained to roughly 5–6 Å to enable bridging by Cd^{2+} ions, in accordance with the metalloprotein database (Castagnetto et al., 2002). (e) The S4 segment adopts combined α-helical and 3_{10}-helix conformations, as indicated by available crystal structures and different modeling studies (Long et al., 2007; Clayton et al., 2008; Villalba-Galea et al., 2008; Bjelkmar et al., 2009; Khalili-Araghi et al., 2010; Vargas et al., 2011; Yarov-Yarovoy et al., 2012).

KCNQ2 model of the open state O

In the open-state model (Fig. 9 D), the 3_{10} helix extends from I205 to R214 (Figs. 8 G and S5 B). As suggested previously (Miceli et al., 2008), the third and fourth gating charges in S4, R207 and R210, form salt bridges in S2 with E130 and E140, respectively (Fig. 8 H). The open state is also stabilized by the formation of a salt bridge between D172 in S3 and R213 in S4. In the open-state model, the hydrophobic residue F137 is located between the interacting pairs R207-E130 and R210-E140 (Fig. 8 H).

KCNQ2 model of the deep resting state C3

The C3 deep resting–state model (Fig. 9 A) emerges from the Cd^{2+} bridge formed between C195 in S4 and C106 in S1 (Fig. 8 B). The 3_{10} helix extends from L197 to L203 (Figs. 8 A and S5 B). In this C3 deep resting state, the first and second gating charges, R198 and R201 of S4, form salt bridges with E130 and E140 of S2, respectively (Fig. 8 B). These interactions stabilize the KCNQ2 channel closed C3 state. The interacting pairs R198-E130 and R201-E140 are, respectively, located above and below the highly conserved phenylalanine, F137 (homologous to F290 and F233 of *Shaker* and Kv1.2 channels, respectively). The side chain of F137 faces the inner side of a hydrophobic sealing (Fig. 8 B) that separates the extracellular and intracellular water-accessible crevices of the VSD and forms the charge-transfer center that catalyzes the gating charge movement (Long et al., 2007; Tao et al., 2010). The homologous F290 in *Shaker* was found to control a final gating transition representing only 10–20% of the total gating charge (Lacroix and Bezanilla, 2011).

KCNQ2 model of the intermediate resting state C2

The C2 resting-state model (Fig. 8 B) emerges from the Cd^{2+} bridges formed by the S4–S1 cysteine pair of C198-C106, whose sulfhydryls are located 4.9 Å apart (Fig. 8 D). The 3_{10} helix extends from R201 to R207 (Figs. 8 C and S5 B). In the C2 model, the S4 gating charge R201 is sufficiently close to E130 in S2 to form salt bridges, and

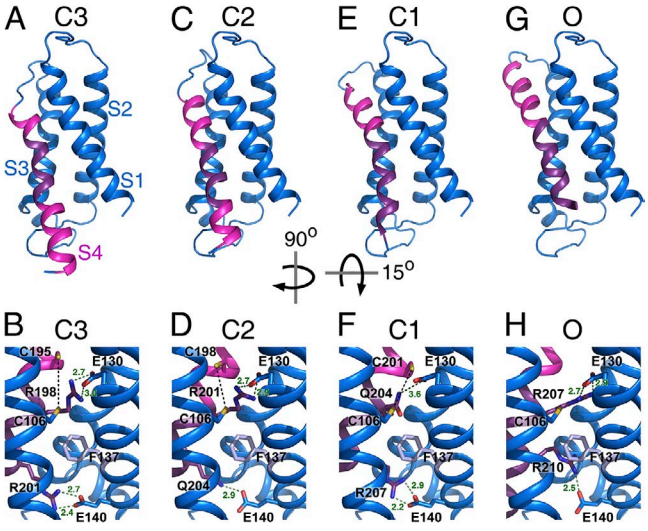

Figure 8. VSDs of KCNQ2 open- and closed-state models. Ribbon diagrams of individual VSDs and their stabilizing interactions, respectively, in: (A and B) the deep resting state C3, (C and D) the intermediate resting state C2, (E and F) the superficial resting state C1, and (G and H) the open state. The S4 α helix is colored in magenta, and the 3_{10}-helix portion is colored in dark magenta. The bottom panels show the cysteine pairs that are sufficiently close to each other to form Cd^{2+} bridges (dashed black lines) and the potential interactions between the S4 and S2 segments. The distances provided inside the panels are in angstrom.

the glutamine residue Q204 in S4 is at hydrogen-bonding distance from E140 in S2 (Fig. 8 D). In the C2 model, the hydrophobic residue F137 spatially separates between the interacting pairs R201-E130 and Q204-E140.

KCNQ2 model of the superficial resting state C1

The C1 resting-state model (Fig. 9 C) emerges from the Cd^{2+} bridges formed by the S4–S1 cysteine pair of C201-C106, whose sulfhydryls are located 5.4 Å apart (Fig. 8 F). The 3_{10} helix extends from L203 to R213 (Figs. 8 E and S5 B). The third gating charge, R207 in S4, is sufficiently close to E140 in S2 to form a salt bridge (Fig. 8 F). In the C1 resting-state model, the hydrophobic residue F137 is located between the interacting pairs Q204-E130 and R207-E140.

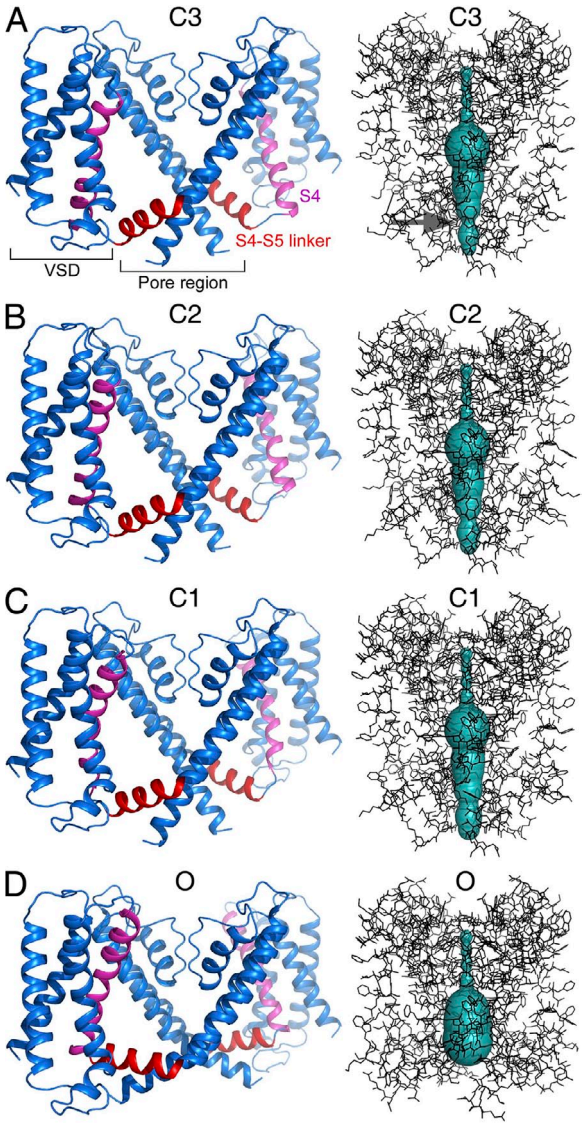

Figure 9. Homology models of KCNQ2 channel open and closed states. (Left) Side views of ribbon diagrams of two facing subunits showing the pore-forming region and the VSD for: (A) the deep resting state C3, (B) the intermediate resting state C2, (C) the superficial resting state C1, and (D) the open state. The rare and frontal subunits were removed for clarity. (Right) Stick models of the channel pore region (black) and the corresponding Voronoi diagrams (bluish-green), as generated for the pore molecular surface from the predicted place of the uppermost K^+ ion down to the bottom of the pore (prepared by MOLE 2.0). The diameter of the pore at the activation gate (level of A317, as indicated in A by a gray arrow) was calculated by MOLE 2.0 as (A) 3.0 Å, (B) 3.6 Å, and (C) 4.5 Å. For the open state (D), the diameter was calculated as 11.4 Å at the level of G310.

Do KCNQ2 C3, C2, and C1 closed states meet with the emerging consensus of VSD resting-state models?

The lack of high resolution atomic structure of a VSD in the resting state has motivated different laboratories to integrate and translate a large body of experimental data into structural information using various modeling approaches. All resting-state models posit that S4 undergoes a rotation and an inward translation along its main axis relatively to the VSD-activated conformation in crystal structures, whereas the S1 and S2 helices do not move during the closed to open transition (Vargas et al., 2011, 2012). This view supports a sliding helix model of the voltage-dependent gating in which the gating-charged arginines in S4 are suggested to sequentially form ion pairs with negatively charged residues in S2–S3 segments during activation of the channel. The models also incorporate the existence of multiple resting states, which are supported by a wide range of experimental data (DeCaen et al., 2009, 2011; Henrion et al., 2012; Lacroix et al., 2012; Vargas et al., 2012; Yarov-Yarovoy et al., 2012).

Our empirical constraints support the existence of multiple KCNQ2 closed states, where the formation of discrete S4–S1 Cd^{2+} bridges capture at least three distinct KCNQ2 resting states: C3, C2, and C1. The KCNQ2 deep resting state C3 model is analogous to the C3 closed state recently described for *Shaker* channels (Henrion et al., 2012), where like in KCNQ2, the S4–S2 interacting pairs R362-E283 and R365-E293 are found above and below the homologous phenylalanine F290, respectively. The importance of the Cd^{2+} bridge formed by C195 in S4 and C106 in S1, which traps the VSD in C3, is underscored by recent models developed for the bacterial voltage-gated Na^+ channel NaChBac (DeCaen et al., 2011; Yarov-Yarovoy et al., 2012). In NaChBac, the outermost S4 residue T110 (also called T0; analogous to S195 in KCNQ2) interacts with E43 at the extracellular end of S1 to stabilize a deep closed state. Although not identical, the deep resting state C3 of KCNQ2 resembles that of resting state C1 described for NaChBac (Yarov-Yarovoy et al., 2012). The KCNQ2 resting-state C2 model shares some similarities with the C2 closed state described by Henrion et al. (2012) for *Shaker* channels. However, there are substantial differences between KCNQ2 and *Shaker*. In the C2 closed state of the *Shaker* channel, the S4–S2 interacting pairs R365-E283 and R368-E293 form salt bridges. In contrast, in KCNQ2, the homologous residue of R368 in S4 is a glutamine,

Q204, which cannot engage into salt bridge with E140 in S2 (E293 in *Shaker*), but probably forms a hydrogen bond with E140. Notably, the experimental data clearly indicate that the ion pair R201-E130 is much more critical for stabilizing a closed-channel conformation than the ion pair R198-E130 because, unlike the R198C mutant, the R201C mutation yields constitutively open channels. The C1 models of KCNQ2 and the *Shaker* channel differ in terms of ion pairing. Although the *Shaker* C1 model assumes two ion pairs (Henrion et al., 2012), in KCNQ2 there is only one ion pairing (R207-E140) and a potential Q204-E130 hydrogen bonding (Fig. 8 F). Interestingly, in silico replacement of C201 by an arginine in model C1 suggests that R201 can potentially interact with E130 also in the superficial C1 resting state (and not only in the intermediate C2 resting state). This possibility may explain the critical role of R201 in stabilizing WT KCNQ channels in a superficial C1 resting state.

Collectively, this study reveals that residue C106 in S1 can be very close to several N-terminal S4 residues (S195, R198, R201) for stabilizing different KCNQ2 resting states. This is in line with previous studies performed in *Shaker* channels showing that the analogous S1 position I241 constrains the resting state of S4 with respect to S1 by interacting with R362 (analogous to R198 in KCNQ2) (Campos et al., 2007). A more recent work also disclosed the importance of this residue for both the VSD movement and its coupling to the pore domain, as mutant I241W could trap the VSD in an intermediate state (Vargas et al., 2012). Our data confirm the importance of residue R201 (R2) in stabilizing the resting state of KCNQ2 by engaging into ion pairing with E130 in S2 (Miceli et al., 2008). Finally, this work shows that despite certain differences, the KCNQ2 resting-state models meet with the emerging consensual VSD resting-state models of Kv channels.

We thank Dr. Thomas Jentsch (Leibniz-Institut für Molekulare Pharmakologie and Max-Delbrück-Centrum für Molekulare Medizin, Berlin) for the human clones of KCNQ2.

This work was supported by the Deutsch-Israelische Projektkooperation fund (DFG, AT 119/1-1 to B. Attali) and by the Wolfson Family Foundation and Israel Science Foundation (grants 812/07 and 1645/07 to Y. Paas).

The authors declare no competing financial interests.

Kenton J. Swartz served as editor.

Submitted: 27 April 2014
Accepted: 15 October 2014

REFERENCES

Armstrong, C.M., and F. Bezanilla. 1974. Charge movement associated with the opening and closing of the activation gates of the Na channels. *J. Gen. Physiol.* 63:533–552. http://dx.doi.org/10.1085/jgp.63.5.533

Berka, K., O. Hanák, D. Sehnal, P. Banás, V. Navrátilová, D. Jaiswal, C.M. Ionescu, R. Svobodová Vareková, J. Koca, and M. Otyepka. 2012. MOLEonline 2.0: interactive web-based analysis of biomacromolecular channels. *Nucleic Acids Res.* 40:W222–W227. http://dx.doi.org/10.1093/nar/gks363

Bjelkmar, P., P.S. Niemelä, I. Vattulainen, and E. Lindahl. 2009. Conformational changes and slow dynamics through microsecond polarized atomistic molecular simulation of an integral Kv1.2 ion channel. *PLOS Comput. Biol.* 5:e1000289. http://dx.doi.org/10.1371/journal.pcbi.1000289

Campos, F.V., B. Chanda, B. Roux, and F. Bezanilla. 2007. Two atomic constraints unambiguously position the S4 segment relative to S1 and S2 segments in the closed state of Shaker K channel. *Proc. Natl. Acad. Sci. USA.* 104:7904–7909. http://dx.doi.org/10.1073/pnas.0702638104

Castagnetto, J.M., S.W. Hennessy, V.A. Roberts, E.D. Getzoff, J.A. Tainer, and M.E. Pique. 2002. MDB: the Metalloprotein Database and Browser at The Scripps Research Institute. *Nucleic Acids Res.* 30:379–382. http://dx.doi.org/10.1093/nar/30.1.379

Catterall, W.A. 2010. Ion channel voltage sensors: Structure, function, and pathophysiology. *Neuron.* 67:915–928. http://dx.doi.org/10.1016/j.neuron.2010.08.021

Clayton, G.M., S. Altieri, L. Heginbotham, V.M. Unger, and J.H. Morais-Cabral. 2008. Structure of the transmembrane regions of a bacterial cyclic nucleotide-regulated channel. *Proc. Natl. Acad. Sci. USA.* 105:1511–1515. http://dx.doi.org/10.1073/pnas.0711533105

DeCaen, P.G., V. Yarov-Yarovoy, E.M. Sharp, T. Scheuer, and W.A. Catterall. 2009. Sequential formation of ion pairs during activation of a sodium channel voltage sensor. *Proc. Natl. Acad. Sci. USA.* 106:22498–22503. http://dx.doi.org/10.1073/pnas.0912307106

DeCaen, P.G., V. Yarov-Yarovoy, T. Scheuer, and W.A. Catterall. 2011. Gating charge interactions with the S1 segment during activation of a Na^+ channel voltage sensor. *Proc. Natl. Acad. Sci. USA.* 108:18825–18830. http://dx.doi.org/10.1073/pnas.1116449108

Delmas, P., and D.A. Brown. 2005. Pathways modulating neural KCNQ/M (Kv7) potassium channels. *Nat. Rev. Neurosci.* 6:850–862. http://dx.doi.org/10.1038/nrn1785

Doyle, D.A., J. Morais Cabral, R.A. Pfuetzner, A. Kuo, J.M. Gulbis, S.L. Cohen, B.T. Chait, and R. MacKinnon. 1998. The structure of the potassium channel: Molecular basis of K^+ conduction and selectivity. *Science.* 280:69–77. http://dx.doi.org/10.1126/science.280.5360.69

Emsley, P., B. Lohkamp, W.G. Scott, and K. Cowtan. 2010. Features and development of *Coot. Acta Crystallogr. D Biol. Crystallogr.* 66:486–501. http://dx.doi.org/10.1107/S0907444910007493

Gibor, G., D. Yakubovich, A. Peretz, and B. Attali. 2004. External barium affects the gating of KCNQ1 potassium channels and produces a pore block via two discrete sites. *J. Gen. Physiol.* 124:83–102. http://dx.doi.org/10.1085/jgp.200409068

Haitin, Y., I. Yisharel, E. Malka, L. Shamgar, H. Schottelndreier, A. Peretz, Y. Paas, and B. Attali. 2008. S1 constrains S4 in the voltage sensor domain of Kv7.1 K^+ channels. *PLoS ONE.* 3:e1935.

Henrion, U., J. Renhorn, S.I. Börjesson, E.M. Nelson, C.S. Schwaiger, P. Bjelkmar, B. Wallner, E. Lindahl, and F. Elinder. 2012. Tracking a complete voltage-sensor cycle with metal-ion bridges. *Proc. Natl. Acad. Sci. USA.* 109:8552–8557. http://dx.doi.org/10.1073/pnas.1116938109

Jensen, M.O., V. Jogini, D.W. Borhani, A.E. Leffler, R.O. Dror, and D.E. Shaw. 2012. Mechanism of voltage gating in potassium channels. *Science.* 336:229–233. http://dx.doi.org/10.1126/science.1216533

Jiang, Y., A. Lee, J. Chen, V. Ruta, M. Cadene, B.T. Chait, and R. MacKinnon. 2003. X-ray structure of a voltage-dependent K^+ channel. *Nature.* 423:33–41. http://dx.doi.org/10.1038/nature01580

Kang, C., C. Tian, F.D. Sönnichsen, J.A. Smith, J. Meiler, A.L. George Jr., C.G. Vanoye, H.J. Kim, and C.R. Sanders. 2008. Structure of KCNE1 and implications for how it modulates the

KCNQ1 potassium channel. *Biochemistry.* 47:7999–8006. http://dx.doi.org/10.1021/bi800875q

Khalili-Araghi, F., V. Jogini, V. Yarov-Yarovoy, E. Tajkhorshid, B. Roux, and K. Schulten. 2010. Calculation of the gating charge for the Kv1.2 voltage-activated potassium channel. *Biophys. J.* 98: 2189–2198. http://dx.doi.org/10.1016/j.bpj.2010.02.056

Lacroix, J.J., and F. Bezanilla. 2011. Control of a final gating charge transition by a hydrophobic residue in the S2 segment of a K^+ channel voltage sensor. *Proc. Natl. Acad. Sci. USA.* 108:6444–6449. http://dx.doi.org/10.1073/pnas.1103397108

Lacroix, J.J., S.A. Pless, L. Maragliano, F.V. Campos, J.D. Galpin, C.A. Ahern, B. Roux, and F. Bezanilla. 2012. Intermediate state trapping of a voltage sensor. *J. Gen. Physiol.* 140:635–652. http://dx.doi.org/10.1085/jgp.201210827

Lainé, M., M.C. Lin, J.P. Bannister, W.R. Silverman, A.F. Mock, B. Roux, and D.M. Papazian. 2003. Atomic proximity between S4 segment and pore domain in Shaker potassium channels. *Neuron.* 39:467–481. http://dx.doi.org/10.1016/S0896-6273(03)00468-9

Li, Y., N. Gamper, D.W. Hilgemann, and M.S. Shapiro. 2005. Regulation of Kv7 (KCNQ) K^+ channel open probability by phosphatidylinositol 4,5-bisphosphate. *J. Neurosci.* 25:9825–9835. http://dx.doi.org/10.1523/JNEUROSCI.2597-05.2005

Lin, M.C., J. Abramson, and D.M. Papazian. 2010. Transfer of ion binding site from ether-á-go-go to Shaker: Mg^{2+} binds to resting state to modulate channel opening. *J. Gen. Physiol.* 135:415–431. http://dx.doi.org/10.1085/jgp.200910320

Lin, M.C., J.Y. Hsieh, A.F. Mock, and D.M. Papazian. 2011. R1 in the Shaker S4 occupies the gating charge transfer center in the resting state. *J. Gen. Physiol.* 138:155–163. http://dx.doi.org/10.1085/jgp.201110642

Long, S.B., E.B. Campbell, and R. Mackinnon. 2005. Crystal structure of a mammalian voltage-dependent Shaker family K^+ channel. *Science.* 309:897–903. http://dx.doi.org/10.1126/science.1116269

Long, S.B., X. Tao, E.B. Campbell, and R. MacKinnon. 2007. Atomic structure of a voltage-dependent K^+ channel in a lipid membrane-like environment. *Nature.* 450:376–382. http://dx.doi.org/10.1038/nature06265

Ma, D., T.S. Tillman, P. Tang, E. Meirovitch, R. Eckenhoff, A. Carnini, and Y. Xu. 2008. NMR studies of a channel protein without membranes: Structure and dynamics of water-solubilized KcsA. *Proc. Natl. Acad. Sci. USA.* 105:16537–16542. http://dx.doi.org/10.1073/pnas.0805501105

Maljevic, S., T.V. Wuttke, and H. Lerche. 2008. Nervous system K_V7 disorders: breakdown of a subthreshold brake. *J. Physiol.* 586:1791–1801. http://dx.doi.org/10.1113/jphysiol.2008.150656

Meisel, E., M. Dvir, Y. Haitin, M. Giladi, A. Peretz, and B. Attali. 2012. KCNQ1 channels do not undergo concerted but sequential gating transitions in both the absence and the presence of KCNE1 protein. *J. Biol. Chem.* 287:34212–34224. http://dx.doi.org/10.1074/jbc.M112.364901

Miceli, F., M.V. Soldovieri, C.C. Hernandez, M.S. Shapiro, L. Annunziato, and M. Taglialatela. 2008. Gating consequences of charge neutralization of arginine residues in the S4 segment of $K_V7.2$, an epilepsy-linked K^+ channel subunit. *Biophys. J.* 95:2254–2264. http://dx.doi.org/10.1529/biophysj.107.128371

Pathak, M.M., V. Yarov-Yarovoy, G. Agarwal, B. Roux, P. Barth, S. Kohout, F. Tombola, and E.Y. Isacoff. 2007. Closing in on the resting state of the Shaker K^+ channel. *Neuron.* 56:124–140. http://dx.doi.org/10.1016/j.neuron.2007.09.023

Payandeh, J., T. Scheuer, N. Zheng, and W.A. Catterall. 2011. The crystal structure of a voltage-gated sodium channel. *Nature.* 475: 353–358. http://dx.doi.org/10.1038/nature10238

Peretz, A., L. Pell, Y. Gofman, Y. Haitin, L. Shamgar, E. Patrich, P. Kornilov, O. Gourgy-Hacohen, N. Ben-Tal, and B. Attali. 2010. Targeting the voltage sensor of Kv7.2 voltage-gated K^+ channels with a new gating-modifier. *Proc. Natl. Acad. Sci. USA.* 107:15637–15642. http://dx.doi.org/10.1073/pnas.0911294107

Peroz, D., N. Rodriguez, F. Choveau, I. Baró, J. Mérot, and G. Loussouarn. 2008. Kv7.1 (KCNQ1) properties and channelopathies. *J. Physiol.* 586:1785–1789. http://dx.doi.org/10.1113/jphysiol.2007.148254

Petřek, M., P. Kosinová, J. Koca, and M. Otyepka. 2007. MOLE: A Voronoi diagram-based explorer of molecular channels, pores, and tunnels. *Structure.* 15:1357–1363. http://dx.doi.org/10.1016/j.str.2007.10.007

Rulíšek, L., and J. Vondrásek. 1998. Coordination geometries of selected transition metal ions (Co^{2+}, Ni^{2+}, Cu^{2+}, Zn^{2+}, Cd^{2+}, and Hg^{2+}) in metalloproteins. *J. Inorg. Biochem.* 71:115–127. http://dx.doi.org/10.1016/S0162-0134(98)10042-9

Schmidt, D., Q.X. Jiang, and R. MacKinnon. 2006. Phospholipids and the origin of cationic gating charges in voltage sensors. *Nature.* 444:775–779. http://dx.doi.org/10.1038/nature05416

Smith, J.A., C.G. Vanoye, A.L. George Jr., J. Meiler, and C.R. Sanders. 2007. Structural models for the KCNQ1 voltage-gated potassium channel. *Biochemistry.* 46:14141–14152. http://dx.doi.org/10.1021/bi701597s

Soldovieri, M.V., F. Miceli, and M. Taglialatela. 2011. Driving with no brakes: Molecular pathophysiology of Kv7 potassium channels. *Physiology (Bethesda).* 26:365–376. http://dx.doi.org/10.1152/physiol.00009.2011

Swartz, K.J. 2004. Towards a structural view of gating in potassium channels. *Nat. Rev. Neurosci.* 5:905–916. http://dx.doi.org/10.1038/nrn1559

Swartz, K.J. 2008. Sensing voltage across lipid membranes. *Nature.* 456:891–897. http://dx.doi.org/10.1038/nature07620

Takeshita, K., S. Sakata, E. Yamashita, Y. Fujiwara, A. Kawanabe, T. Kurokawa, Y. Okochi, M. Matsuda, H. Narita, Y. Okamura, and A. Nakagawa. 2014. X-ray crystal structure of voltage-gated proton channel. *Nat. Struct. Mol. Biol.* 21:352–357. http://dx.doi.org/10.1038/nsmb.2783

Tao, X., A. Lee, W. Limapichat, D.A. Dougherty, and R. MacKinnon. 2010. A gating charge transfer center in voltage sensors. *Science.* 328:67–73. http://dx.doi.org/10.1126/science.1185954

Van Horn, W.D., C.G. Vanoye, and C.R. Sanders. 2011. Working model for the structural basis for KCNE1 modulation of the KCNQ1 potassium channel. *Curr. Opin. Struct. Biol.* 21:283–291. http://dx.doi.org/10.1016/j.sbi.2011.01.001

Vargas, E., F. Bezanilla, and B. Roux. 2011. In search of a consensus model of the resting state of a voltage-sensing domain. *Neuron.* 72:713–720. http://dx.doi.org/10.1016/j.neuron.2011.09.024

Vargas, E., V. Yarov-Yarovoy, F. Khalili-Araghi, W.A. Catterall, M.L. Klein, M. Tarek, E. Lindahl, K. Schulten, E. Perozo, F. Bezanilla, and B. Roux. 2012. An emerging consensus on voltage-dependent gating from computational modeling and molecular dynamics simulations. *J. Gen. Physiol.* 140:587–594. http://dx.doi.org/10.1085/jgp.201210873

Villalba-Galea, C.A., W. Sandtner, D.M. Starace, and F. Bezanilla. 2008. S4-based voltage sensors have three major conformations. *Proc. Natl. Acad. Sci. USA.* 105:17600–17607. http://dx.doi.org/10.1073/pnas.0807387105

Webster, S.M., D. Del Camino, J.P. Dekker, and G. Yellen. 2004. Intracellular gate opening in Shaker K^+ channels defined by high-affinity metal bridges. *Nature.* 428:864–868. http://dx.doi.org/10.1038/nature02468

Weckhuysen, S., S. Mandelstam, A. Suls, D. Audenaert, T. Deconinck, L.R. Claes, L. Deprez, K. Smets, D. Hristova, I. Yordanova, et al. 2012. KCNQ2 encephalopathy: Emerging phenotype of a neonatal epileptic encephalopathy. *Ann. Neurol.* 71:15–25. http://dx.doi.org/10.1002/ana.22644

Xu, X., M. Jiang, K.L. Hsu, M. Zhang, and G.N. Tseng. 2008. KCNQ1 and KCNE1 in the IKs channel complex make state-dependent contacts in their extracellular domains. *J. Gen. Physiol.* 131:589–603. http://dx.doi.org/10.1085/jgp.200809976

Xu, Y., Y. Wang, X.Y. Meng, M. Zhang, M. Jiang, M. Cui, and G.N. Tseng. 2013. Building KCNQ1/KCNE1 channel models and probing their interactions by molecular-dynamics simulations. *Biophys. J.* 105:2461–2473. http://dx.doi.org/10.1016/j.bpj.2013.09.058

Yarov-Yarovoy, V., P.G. DeCaen, R.E. Westenbroek, C.Y. Pan, T. Scheuer, D. Baker, and W.A. Catterall. 2012. Structural basis for gating charge movement in the voltage sensor of a sodium channel. *Proc. Natl. Acad. Sci. USA.* 109:E93–E102. http://dx.doi.org/10.1073/pnas.1118434109

Yellen, G. 1998. The moving parts of voltage-gated ion channels. *Q. Rev. Biophys.* 31:239–295. http://dx.doi.org/10.1017/S0033583598003448